

## Refractive Index of Engine-Emitted Black Carbon and the Influence of Organic Coatings on Optical Properties

Dawei Hu, M. Rami Alfarra, Kate Szpek, Justin M. Langridge, Michael I. Cotterell, Michael J. Flynn, Yunqi Shao, Aristeidis Voliotis, Mao Du, Dantong Liu, Ben Johnson, Gordon McFiggans, Jim M. Haywood, Hugh Coe, James Allan

### Item type

Journal Contribution

### Terms of use

This work is licensed under a [CC BY 4.0](https://creativecommons.org/licenses/by/4.0/) license

### This version is available at

[https://manara.qnl.qa/articles/journal\\_contribution/Refractive\\_Index\\_of\\_Engine\\_Emitted\\_Black\\_Carbon\\_and\\_the\\_Influence\\_of\\_Or](https://manara.qnl.qa/articles/journal_contribution/Refractive_Index_of_Engine_Emitted_Black_Carbon_and_the_Influence_of_Or)

Access the item on Manara for more information about usage details and recommended citation.

Posted on Manara – Qatar Research Repository on

2023-08-12



## RESEARCH ARTICLE

10.1029/2023JD039178

## Key Points:

- Refractive indices of BC/BrC were derived without multiple charge artifacts
- A single RI may be sufficient for simulating the radiative forcing of secondary organic aerosol particles at the wavelength of 660 nm
- Considering morphology may be necessary for accurate predictions of the absorption of coated BC particles

## Supporting Information:

Supporting Information may be found in the online version of this article.

## Correspondence to:

D. Hu and J. Allan,  
dawei.hu@manchester.ac.uk;  
james.allan@manchester.ac.uk

## Citation:

Hu, D., Alfarra, M. R., Szpek, K., Langridge, J. M., Cotterell, M. I., Flynn, M. J., et al. (2023). Refractive index of engine-emitted black carbon and the influence of organic coatings on optical properties. *Journal of Geophysical Research: Atmospheres*, 128, e2023JD039178. <https://doi.org/10.1029/2023JD039178>

Received 28 APR 2023

Accepted 12 AUG 2023

## Refractive Index of Engine-Emitted Black Carbon and the Influence of Organic Coatings on Optical Properties

Dawei Hu<sup>1</sup> , M. Rami Alfarra<sup>1,2,3</sup> , Kate Szpek<sup>4</sup> , Justin M. Langridge<sup>4</sup> , Michael I. Cotterell<sup>5</sup> , Michael J. Flynn<sup>1</sup>, Yunqi Shao<sup>1</sup>, Aristeidis Voliotis<sup>1</sup> , Mao Du<sup>1,6</sup>, Dantong Liu<sup>7</sup> , Ben Johnson<sup>4</sup> , Gordon McFiggans<sup>1</sup>, Jim M. Haywood<sup>4,8</sup> , Hugh Coe<sup>1</sup>, and James Allan<sup>1,2</sup>
<sup>1</sup>Department of Earth and Environmental Sciences, University of Manchester, Manchester, UK, <sup>2</sup>National Centre for Atmospheric Science, University of Manchester, Manchester, UK, <sup>3</sup>Now at Qatar Environment and Energy Research Institute, Hamad Bin Khalifa University (HBKU), Doha, Qatar, <sup>4</sup>Met Office, Exeter, UK, <sup>5</sup>School of Chemistry, University of Bristol, Bristol, UK, <sup>6</sup>Now at School of Geography Earth and Environment Sciences, University of Birmingham, Birmingham, UK, <sup>7</sup>Department of Atmospheric Sciences, School of Earth Sciences, Zhejiang University, Hangzhou, China, <sup>8</sup>College for Engineering, Mathematics and Physical Sciences, University of Exeter, Exeter, UK

**Abstract** Refractive indices (RI) of particles are important in determining their radiative forcing. We measured optical coefficients of particles classified according to their aerodynamic diameter, allowing retrieval of RI using a Mie model. At 405 nm, the RI of BC from a diesel engine was  $1.870 (\pm 0.132) + 0.640 (\pm 0.015) i$ . The RI of secondary organic aerosol (SOA), using  $\alpha$ -pinene and o-cresol as precursors, were  $1.584 \pm 0.015$  and  $1.738 (\pm 0.021) + 0.0316 (\pm 0.0018) i$ , respectively. Neither SOAs demonstrated absorption at 660 nm and their RIs were  $1.551 \pm 0.011$  and  $1.586 \pm 0.011$ , the similar value suggesting that a single RI may be sufficient for simulating the radiative forcing of SOA at this wavelength. In addition, organics were condensed onto BC to test optical models for coated particles. For BC particles coated with non-absorbing organics, the extinction is predicted accurately by all models. The absorption is significantly over-estimated by core-shell, volume mixing, and effective medium approximations and under-estimated by external mixing. For BC particles coated with weakly absorbing organics, the extinction and absorption are best described by external mixing when the coating ratio is less than 2.5. When the coating ratio is over 2.5, the difference between the external mixing predictions and measurements increases with the coating ratio. Our results show that the absorption of coated BC particles may not be predicted accurately based solely on the equivalent diameter, coating ratio, and pure component RIs, and considerations of additional factors such as morphology may be necessary.

**Plain Language Summary** Black carbon (BC) and brown carbon (BrC) are extensively investigated components of atmospheric aerosol due to their ability to absorb solar radiation and contribute to atmospheric heating, resulting in a positive radiative forcing. Although BC and BrC are very important for climate, they are poorly represented in atmospheric models. This is in part due to the lack of accurate refractive index (RI) descriptions for both BC and BrC. Previous studies have used mobility selection approaches to select BC/BrC particles upstream of optical spectroscopy instruments to allow RI characterizations, but these retrievals suffer from issues caused by multiple charging. We solved this issue by using a new aerosol classification technique, enabling optical measurements for an aerosol sample classified according to a single physical size without multiple charge artifacts, which improves the subsequent RI retrieval. In addition, non-absorbing and weakly absorbing organic materials were condensed onto BC to form coated soot particles, allowing different optical models for mixed particles to be evaluated. We found that the absorption of coated BC particles may not be predicted with sufficient accuracy from knowledge of only the equivalent diameter, coating composition, and RI, and considering additional factors such as morphology may be necessary for accurate predictions.

## 1. Introduction

Black carbon (BC) is a closely investigated component of atmospheric aerosol because it absorbs solar radiation and heats the atmosphere thereby causing a positive radiative forcing of climate (Bond & Bergstrom, 2006a; Bond et al., 2013; Haywood and Shine, 1995; Liu et al., 2020a). BC is emitted through incomplete combustion processes, originating from both anthropogenic (e.g., diesel engines) and natural (e.g., wildfires) sources. After emission into the atmosphere, inorganic and organic materials often condense onto BC particulates through atmospheric aging processes. The resulting absorption cross sections of the BC particles are enhanced by these

© 2023. The Authors.

This is an open access article under the terms of the [Creative Commons Attribution License](#), which permits use, distribution and reproduction in any medium, provided the original work is properly cited.

coatings, including through the so-called “lensing effect” (Cappa et al., 2019; Liu et al., 2015, 2017; Sedlacek et al., 2022; Taylor et al., 2020; Wu et al., 2021; Zhang et al., 2017, 2018). Although BC particles exert a strong radiative forcing on climate (IPCC, 2022), climate models often employ simplified BC representations that contribute to uncertainty in radiative forcing impacts that could be improved through better process representation (Zuidema et al., 2016). The use of simplistic representations of aerosols is, in part, necessitated by a lack of accurate refractive index (RI) descriptions for BC and a poor understanding of the impact of coating materials on particle absorption (Liu et al., 2020b), together with uncertainties in modeling the horizontal spatial distribution and vertical profile of aerosols relative to clouds (Haywood et al., 2021; Zuidema et al., 2016).

The conventional approach to retrieve the RI of BC is to remove any coating materials and then measure the optical properties for particles with a classified size or mass (Moteki et al., 2010). Previous studies have often utilized a thermal denuder (TD) to remove coating materials (Knox et al., 2009; Liu et al., 2015) and a differential mobility analyzer (DMA) to classify charged aerosols based on their electrical mobility diameter (Cotterell et al., 2020). However, low-volatility compounds are not removed at common TD operating temperatures (150–300°C) (Shetty et al., 2021). If higher temperatures are used, many atmospheric particulate organic compounds char rather than volatilize (Cavalli et al., 2010). Meanwhile, the DMA approach to particle classification suffers from multiple charge “artifacts,” with the classified aerosol sample being highly polydisperse and the particle size distribution comprising multiple modes (Cotterell et al., 2020). Although the multiple charging effects can be accounted in optical calculations, the residual uncertainties in the particle size distribution still affect model calculations of the particle optical properties. These uncertainties in coating content and particle size distribution can lead to large uncertainties in the determined RI for BC. To solve these problems, the Soot Aerodynamic Size Selection for Optical properties (SASSO) project used an Aerodynamic Aerosol Classifier (AAC) for monomodal particle size classification and interrogated fresh BC particles for which the condensation of volatile coatings was prevented. The latter was achieved by passing the emissions from the exhaust of a hot diesel engine immediately through a heated dilutor (140°C, with hot dilution air at 140°C) followed by a catalytic stripper (operating at 350°C) before introducing them into the chamber. The hot dilutor ensures that VOCs remain in the gas phase, while the catalytic stripper removes the gas-phase VOCs and any residual condensed phase organics to ensure the BC particles have no coatings. The AAC classifies particles according to aerodynamic diameter for subsequent size and mass distribution measurements and optical evaluation (Hu et al., 2021a; Tavakoli et al., 2014), and does not suffer from multiple charge artifacts that affect measurements on mobility-classified particles. Specifically, SASSO has applied the AAC classification of these aerosol emissions prior to optical interrogation using cavity ring-down and photoacoustic spectroscopy with the EXtinction, SCattering and Absorption of Light for AirBorne Aerosol Research (EXSCALABAR) instrument, which is a custom-built suite of laser-based spectrometers with integrated sample conditioning that was developed by the Met Office (Cotterell et al., 2019a, 2020; Davies et al., 2018).

Coatings on BC particles can enhance their per-mass absorption, through the “lensing effect”. However, the effect of coating materials on the absorption properties of BC is still unclear. Many climate models assume aerosols are internally mixed in radiative calculations (Adachi et al., 2010; Johnson et al., 2016; Liu et al., 2015; Martins et al., 1998). However, studies report that the common idealized uniformly mixed and perfectly coated (core-shell) aerosol treatments that are commonly adopted in these models overestimate aerosol absorption enhancement (Cappa et al., 2012). Specifically, uniform mixing treatments produce up to twice the absorption enhancement by the presence of organics in BC particles compared to models that account accurately for the particle mixing states (Fierce et al., 2016). Meanwhile, the core-shell mixing assumption can lead to overestimates of particle absorption by ~30% for non-spherical aerosols with a non-uniform composition (Adachi et al., 2010). Liu et al. (2017) reported that the absorption enhancement of BC particles is dependent on the mass ratio of coatings to BC. When the ratio is less than 1.5, the absorption by the particle may be considered as having no absorption enhancement by the presence of the coating. When this ratio is greater than 3, the absorption is enhanced significantly by optical lensing phenomena. Taylor et al. (2020) compared the measured absorption of highly aged biomass burning smoke with those simulated using several internal mixing optical models (core-shell, volume mixing, Maxwell-Garnett, and Bruggeman), and showed that the homogeneous “gray-sphere” Mie models (using volume mixing, Maxwell-Garnett, or Bruggeman approximations for the refractive index) were unable to predict BC absorption, while the core-shell Mie model predicted accurately the BC absorption at long visible wavelengths (>514 nm) but failed at short visible wavelengths. A better understanding and implementation of the absorption enhancement of BC particles by non- or weakly absorbing coatings and the accuracy of optical model treatments is needed to improve the climate model simulations.

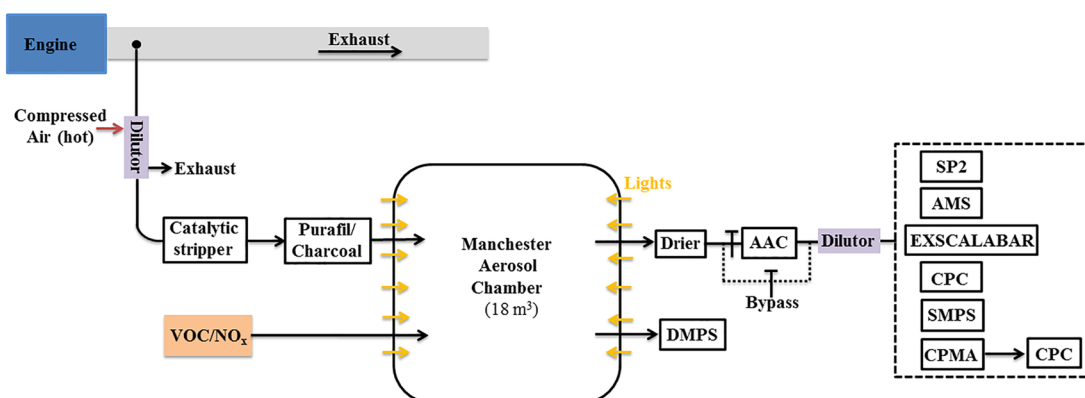


**Figure 1.** Schematic diagram of the experimental configuration.

The purpose of this paper is to: (a) retrieve accurate RI values of pure BC particles emitted from a diesel engine and the RI of non- or weakly absorbing SOA formed through photochemical reactions in the laboratory; and (b) investigate the optical properties for mixed aerosol particles formed by condensing non- or weakly absorbing SOA onto BC, and critically test different models (external mixing, core-shell, a linear volume-weighted mixing rule, and effective medium approximations that include both Maxwell-Garnett and Bruggeman's rules) of the optical properties of mixed particles. This work provides fundamental underpinning information needed to improve the prediction of the radiative forcing of BC and BrC in the atmosphere. The work presented here builds on the results reported in our previous publication (Hu et al., 2021a), which described our experimental apparatus, aerosol generation, and conditioning methods, and the chemical and morphological characterization of the particles, but did not investigate the optical properties.

## 2. Experimental Setup and Methods

This study uses data from the Manchester diesel engine and aerosol chamber experiments described by Hu et al. (2021a). Figure 1 shows the instrument configuration during SASSO. In this study, several instruments sampled the size-selected aerosols downstream of an AAC. A Scanning Mobility Particle Sizer (SMPS) and Centrifugal Particle Mass Analyzer (CPMA) measured the mobility size and mass distributions of the particles, respectively. The Single Particle Soot Photometer (SP2) and AMS measured the refractory black carbon (rBC) core size distribution and chemical composition of the aerosols, respectively. EXSCALABAR measured the absorption and extinction coefficients of the AAC-selected aerosols.

The advantages of this setup are: (a) VOCs were prevented from condensing onto BC particles by using a hot dilutor followed by a catalytic stripper, and (b) The particle size distribution and optical properties were characterized for AAC-selected particles, with this approach not subject to multiple charge artifacts that disadvantage approaches that use electrical mobility classification. The experimental procedure and the principal of the instruments has been described in detail in Hu et al. (2021a) and only a brief description is given below.

### 2.1. Instrumentation

#### 2.1.1. Aerodynamic Aerosol Classifier

The AAC (Cambustion Ltd, Cambridge, UK) is utilized to select aerosols within a narrow range of aerodynamic diameters. This instrument employs the principles of centrifugal force and sheath flow between two concentric rotating cylinders to classify the aerosol based on its aerodynamic diameter. The principles of aerodynamic size selection using the AAC are outlined in Tavakoli et al. (2014).

#### 2.1.2. EXtinction, SCattering and Absorption of Light for AirBorne Aerosol Research (EXSCALABAR)

EXSCALABAR is a bespoke aerosol optical spectroscopy instrument. We refer the reader to our previous papers (Cotterell et al., 2019a, 2019b, 2020, 2021; Davies et al., 2018) that describe this instrument thoroughly. In brief, the instrument uses cavity ring-down spectroscopy (CRDS) to measure extinction coefficients at 405 and 660 nm wavelengths and photoacoustic spectroscopy (PAS) to measure absorption coefficients at the wavelengths of

405, 515, and 660 nm, for dried aerosol particles. For deployment during SASSO, the aerosol sample drawn through each spectrometer shared common sample conditioning; the aerosol sample was initially drawn through a Nafion drier (Perma Pure LLC) to reduce the relative humidity to <10%, and then passed through an activated charcoal “honeycomb” scrubber (custom-built in-house) to remove ozone and NO<sub>x</sub> from the gas phase that would otherwise contribute to light extinction and absorption at the discrete visible wavelengths of our CRDS and PAS spectrometers, respectively. The sample then passed through a custom designed aerodynamic impactor with an aerodynamic cut-off diameter (D<sub>50</sub>) of 1.3 μm, before being drawn through a series of flow splitters that distributed the aerosol-laden air samples between the CRDS and PAS spectrometers. The aerosol-laden sample was drawn through each spectrometer at a flow rate of 1 L min<sup>-1</sup>. For both the 405 and 660 nm wavelengths, the PAS spectrometer was mounted immediately downstream of the CRDS spectrometer (CRDS-PAS), that is, the sample passed through the CRDS spectrometer before entering the PAS spectrometer of the same wavelength. All other spectrometers operated in parallel with these. For this study, a Condensation Particle Counter (CPC) (Model 3776, TSI, USA) was fitted in parallel with the sample lines. Automated baseline measurements were made every 10 min by passing the sample through a HEPA filter. The PAS cells were calibrated using ozone before and after each set of experiments and at least once every working week during the experimental periods; this calibration and its accuracy is described by Davies et al. (2018), Cotterell et al. (2019a), and Cotterell et al. (2021).

### 2.1.3. Single Particle Soot Photometer

The size distribution and mass concentration of refractory black carbon (rBC) was quantified using a SP2 (Droplet Measurement Technologies, Colorado, USA). The SP2 utilizes laser-induced incandescence to determine the rBC mass and optical size of individual BC particles. This is achieved by employing an intra-cavity Nd:YAG laser operating at 1064 nm. The particle size can be determined by analyzing the light scattered by particles, where the maximum intensity of scattering is correlated with the optical particle diameter through a calibration using polystyrene latex spheres. The optical size of BC-containing particles is determined by matching the measured scattering signal with calculations based on a core-shell Mie model for light scattering (Moteki and Kondo, 2007; Taylor et al., 2015). When particles contain absorbing materials like refractory BC, they absorb 1,064 nm light, resulting in heating and emission of visible thermal radiation (incandescence). The intensity of this incandescence signal is directly proportional to the mass of rBC, which is determined by a calibration with BC aerosols of known or independently measured mass (Liu et al., 2010).

### 2.1.4. High-Resolution Aerosol Mass Spectrometer (HR-AMS)

Real-time measurements of non-refractory aerosol chemical abundances, including sulfate, nitrate, ammonium, chloride, and organics were conducted using a HR-AMS. The operation and data analysis procedures for the HR-AMS have been described in detail in previous studies (Alfarra et al., 2012; Canagaratna et al., 2007). The ionization efficiency of the AMS was calibrated using monodisperse ammonium nitrate particles.

### 2.1.5. Scanning Mobility Particle Sizer (SMPS)

A commercial SMPS system (TSI, USA) consisting of a 3081 DMA and a 3786 CPC was employed to measure aerosol size distributions in the diameter range of 14.9–673.2 nm. The sheath and sample flow rates were set at 3 L min<sup>-1</sup> and 0.3 L min<sup>-1</sup>, respectively. A bipolar charge distribution was imparted to the aerosol particles entering classifier using a Kr-85 neutralizer. The scan time of the DMA is set to 60 s. During the measurement, the SMPS software (AIM version 10) implemented corrections for both multiple charge effects and diffusion losses. Before the experiment, the SMPS was calibrated using NIST certified polystyrene latex spheres (PSLs, Thermo Fisher Inc.).

### 2.1.6. Differential Mobility Particle Sizer (DMPS)

The size distributions of polydisperse particles formed/introduced in the chamber were directly measured using a custom-built DMPS (consisting of a Brechtel DMA and 3782 CPC). The sheath and sample flow rates were set at 3 L min<sup>-1</sup> and 0.3 L min<sup>-1</sup>, respectively. A bipolar charge distribution was applied to the aerosol particles entering classifier using a Kr-85 neutralizer. The DMA operated in stepping mode, covering the size range of 22–536 nm every 10 min. Before the experiment, the DMPS was calibrated using NIST-certified polystyrene latex spheres (PSLs, Thermo Fisher Inc.).

### 2.1.7. Centrifugal Particle Mass Analyzer (CPMA)

The CPMA (Cambustion Ltd., Cambridge, UK) employs opposing electrical and centrifugal fields to classify particles based on their mass-to-charge ratio. By adjusting the electrical field and rotation speed, particles can

be selected according to their mass. Detailed explanations of the principles and operation of the CPMA can be found in previous studies (Olfert and Collings, 2005; Olfert et al., 2006). The combination of the CPMA with a CPC (Model 3776, TSI, USA) and scanning across the desired mass range enables the determination of bulk aerosol mass size distribution. However, since the CPMA utilizes an electrical classification method, it suffers from multiple charge artifacts and potential transmission issues with uncharged particles, particularly at the lower rotation speeds. In this study, a  $^{90}\text{Sr}$  radioactive ionizer was utilized to neutralize particles prior to their sampling by the CPMA.

### 2.1.8. The Manchester Aerosol Chamber

The Manchester Aerosol Chamber is composed of an  $18\text{ m}^3$  collapsible Teflon bag made of Fluorinated ethylene propylene ( $3\text{ m (H)} \times 3\text{ m (L)} \times 2\text{ m (W)}$ ). It was operated as a batch reactor, providing control over the composition of the gaseous precursors, oxidising environment, primary emissions or seed particles, as well as relative humidity and temperature. Halogen bulbs and two 6 kW xenon arc lamps were mounted on the inside of the enclosure housing the bag, which was coated with a reflective space blanket to optimize irradiance and achieve uniform illumination throughout the chamber. Further details on the chamber are given by Alfarrar et al. (2012). In this study, the chamber was cleaned after each experiment, including several fill–flush cycles of the chamber with clean air, followed by an overnight fill with a high concentration of  $\text{O}_3$  ( $\sim 1\text{ ppm}$ ) to oxidize any residual  $\text{O}_3$ -reactive volatile species. Before the next experiment, additional fill–flush cycles of the chamber with clean air were conducted to ensure a low concentration of pollutants in both gas ( $\text{NO}_x$  concentration less than 10 ppb,  $\text{O}_3$  concentration less than 2 ppb) and particle (number concentration less than  $10/\text{cm}^3$ ) phases.

## 2.2. Particle Generation

### 2.2.1. Bare BC Generation

BC particles were produced from a Volkswagen 1.9 L SDI light duty diesel engine (EURO 4 car equivalent), as used in previous publications (Liu et al., 2017; Pereira et al., 2018). For each experiment, the engine was started and warmed up at 2,000 rpm with 30% load. Once the engine reached a steady temperature (after  $\sim 10\text{ min}$ ), the exhaust was drawn through a pre-heated Dekati DI-1000 ejector dilute (the dilutor was covered by a heated jacket and dilution air was pre-heated to  $140^\circ\text{C}$ ). The sample was then passed through a catalytic stripper (operated at  $350^\circ\text{C}$ , Model CS10, Catalytic Instruments, Germany), a custom-built Purafil (Purafil Inc., USA) and activated charcoal “honeycomb” scrubber to remove any coatings on the BC particles, before entering the Manchester aerosol chamber. In this study, it took around 2 hr of injection to get the desirable BC mass concentration for the monodispersed aerosol absorption measurement.

### 2.2.2. Non- or Weakly Absorbing SOA Formations

To test the absorption enhancement of BC particles by coating materials, two types of SOA were formed in the Manchester aerosol chamber; one non-absorbing and another weakly absorbing (i.e., BrC). The procedures for generating both types of SOA are described in detail in Hu et al. (2021a). Briefly, before the experiment, the chamber was cleaned by several fill/flush cycles with clean air to ensure a low concentration of pollutants in both gas and particle phases. At the beginning of the final fill, the RH of the air inside the chamber was adjusted by passing the clean air through a humidifier. The humidifier generates water vapor by heating ultra-pure water. As the final fill approached its end,  $\text{NO}_2$  [10% v/v, with a balance gas of high purity  $\text{N}_2$  (BOC, UK)] was directly injected into the chamber from a custom-made gas cylinder through stainless steel tubing. The concentration of  $\text{NO}_x$  was measured using a chemi-luminescence gas analyzer (Model 42i, Thermo Scientific, MA, USA). Once the desired  $\text{NO}_x$  concentration was reached in the chamber, the precursor VOC was injected into a heated glass bulb ( $80^\circ\text{C}$ ) and then flushed into the chamber with high-purity nitrogen. In this study, 50 ppb  $\text{NO}_x$  and 250 ppb  $\alpha$ -pinene (Sigma-Aldrich) were used to form the non-absorbing SOA, while 400 ppb o-cresol (Sigma-Aldrich) and 60 ppb  $\text{NO}_x$  were used to form the weakly absorbing BrC. Both experiments were conducted with light irradiation. The irradiation spectrum has been tested approximate the natural atmospheric actinic spectrum. In experiments forming brown carbon SOA, the UV filter from one of the xenon arc lamps was removed to accelerate and enhance the “brown” SOA formation. In experiments where BC particles were coated with SOA, the BC was first injected into the chamber for  $\sim 2\text{ hr}$ . After the BC mass concentration had accumulated to adequate levels in the chamber, the VOC and  $\text{NO}_x$  were injected into the chamber, and organics condensed onto the BC particles after the lights were switched on.



### 2.3. Derivation of Refractive Index

In this study, the refractive indices of aerosol particles were retrieved by comparing the measured absorption and extinction coefficients for size-selected aerosol to predictions using a Mie-based model (Peña and Pal, 2009). We acknowledge that our choice in using Mie theory (which strictly applies to homogeneous spheres only) to retrieve the refractive indices of soot particles likely gives rise to errors in our retrieved RI values. However, the aim of this work is to derive effective RI values for use in climate models, which mostly rely on Mie theory-based models. The extinction and absorption coefficients of the AAC-selected particles were directly measured by CRDS and PAS, respectively. For the Mie prediction, the particle size dependent optical cross-sections were first generated with an initial value of  $RI_{\text{trial}}$  (a complex number i.e., comprised of a real component  $n_{\text{trial}}$  and an imaginary component  $k_{\text{trial}}$ ). These calculated optical cross sections were then integrated over the measured size distribution, weighted for particle number concentration, to give the predicted extinction and absorption coefficients of the aerosol sample. The predicted optical coefficients were then compared to measured values for the initial value of  $RI_{\text{trial}}$  using the least combined squared normalized residual (Equation 1).

$$RSS = \left( \frac{Ext_{\text{pred}} - Ext_{\text{meas}}}{Ext_{\text{meas}}} \right)^2 + \left( \frac{Abs_{\text{pred}} - Abs_{\text{meas}}}{Abs_{\text{meas}}} \right)^2 \quad (1)$$

where RSS is the residual sum of normalized squares,  $Ext_{\text{pred}}$  and  $Abs_{\text{pred}}$  are the predicted extinction and absorption coefficients respectively,  $Ext_{\text{meas}}$  and  $Abs_{\text{meas}}$  are the measured extinction and absorption coefficients respectively.

We iterated over a range of values for  $n_{\text{trial}}$  and  $k_{\text{trial}}$  until the measured optical coefficients and predictions converged such that the difference between the measured and calculated coefficients differed by less than 1%. In addition, methods to analytically estimate errors based on measurement and sizing accuracy were developed and we provide a rigorous analysis of the uncertainties in the refractive index retrievals in Section S1 in Supporting Information S1.

As optical properties depend on the sphere-equivalent volume of the particles, the volume equivalent diameter should be used in the model calculations. For pure SOA particles, with morphology close to spherical (Adachi et al., 2019), the number-based mobility diameter distribution measured by SMPS was used for the optical coefficient calculation. For BC particles, which exist as aggregates of primary spherules and have irregular geometries, the number size distribution measured by the SP2 was used for the optical coefficient calculations. We note that the CPMA-measured mass distributions were not used in optical closure calculations because the CPMA scanning time takes several minutes, and the particle concentration may change during this time and therefore determined size distributions based on an assumed density were not regarded as accurate. Nonetheless, the CPMA was used to calibrate the SP2 for black carbon mass (Hu et al., 2021a) and therefore inclusion of CPMA measurements in our set-up remained highly beneficial.

## 3. Results and Discussion

### 3.1. Refractive Index of Non- or Weakly Absorbing SOA

Figure 2 shows the evolving concentrations of gas pollutants ( $NO_x$  and  $O_3$ ), particle size distribution, and optical properties during the SOA formation experiments. The gray shaded areas are AAC size-selection periods required for refractive index retrievals. The bottom panel in Figure 2 (also in Figure 4) presents the evolution of size distribution of polydisperse particles in the chamber, which was measured by a DMPS sampling directly from the chamber (i.e., without prior AAC selection, see Figure 1). For the non-absorbing SOA formation experiment (Figure 2a), after the precursors ( $\alpha$ -pinene and  $NO_x$ ) were introduced into the chamber and the lights were switched on, the SOA started to be detected after  $\sim 45$  min and the particle size increased to  $\sim 200$  nm over the following 1.5 hr. Over the entire measurement period, there was no detectable aerosol light absorption at either the 405 or 660 nm wavelengths even for the polydisperse particles with high number concentration. The extinction and absorption coefficients below  $1 \text{ Mm}^{-1}$  were assessed to be below the sensitivity thresholds for our CRDS and PAS spectrometers and were therefore removed during data post-processing. Therefore, the SOA formed was non-absorbing in the visible spectrum, consistent with the results reported in previous studies (Nakayama et al., 2010). For the weakly absorbing SOA formation experiment (Figure 2b), after the precursors (cresol and  $NO_x$ ) were introduced into the chamber, the SOA started to be detected just after the lights were

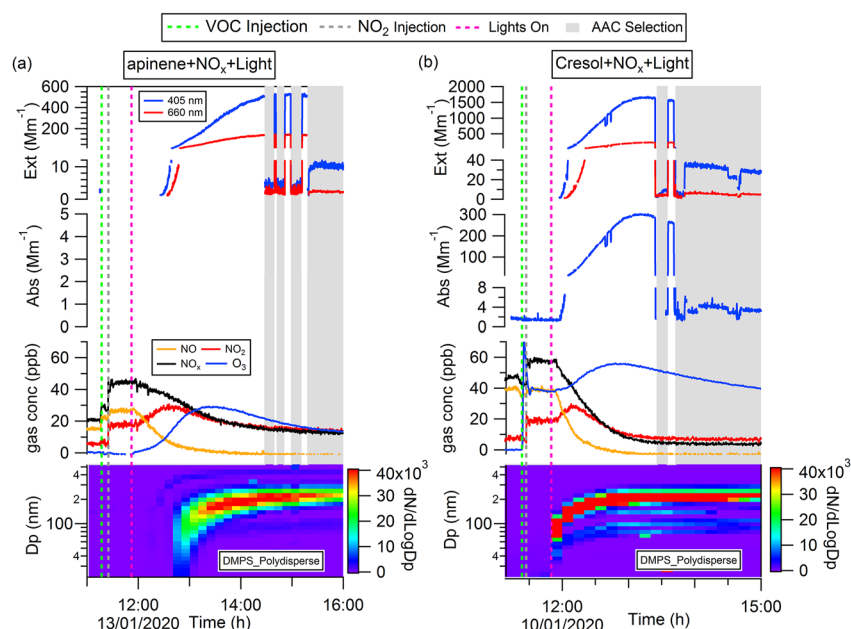


**Figure 2.** Formation and evolution of: (a) the non-absorbing SOA with the precursor of  $\alpha$ -pinene and  $\text{NO}_x$ , and (b) weakly absorbing SOA with the precursor of cresol and  $\text{NO}_x$ , in the chamber. The gray shaded area is AAC selection period. The acronyms Abs, Ext and  $D_p$  are the absorption coefficient, extinction coefficient and mobility diameter of the particles, respectively.

switched on and the particle size increased to  $\sim 200$  nm after  $\sim 40$  min. The faster SOA formation, compared to the non-absorbing SOA formation experiment, may have been caused by the removal of the UV filter from one of the xenon arc lamps during the experiments involving o-cresol. Absorption was observed at the 405 nm wavelength, but not at 660 nm, implying that weakly absorbing SOA (brown carbon) was produced.

Once the SOA particle size stopped increasing, the AAC was used to classify particles according to their aerodynamic diameter for subsequent size distribution and optical properties measurements (gray shaded areas in Figure 2). During the experiments, to get the maximum absorption signal from the AAC-selected particles, the particle aerodynamic size distribution was first scanned by the AAC to find the volume mode aerodynamic diameter. The AAC was then set to this value to classify aerosols for the downstream measurements. The particle absorption coefficient, extinction coefficient, and the average size distribution during the AAC size-selection period are presented in Figure 3. For the non-absorbing SOA (Figure 3a), the number mode average mobility diameter of the AAC-classified particles was  $215.57$  nm, and the total number concentration was  $152 \pm 9$   $\text{cm}^{-3}$ . The corresponding mean extinction coefficients at 405 and 660 nm were  $10.15 \pm 0.15$   $\text{Mm}^{-1}$  and  $2.31 \pm 0.04$   $\text{Mm}^{-1}$ , respectively. No absorption was observed at either wavelength during this experiment. The RI can be retrieved from the full particle number distribution and the average extinction coefficient using the method presented in Section 2.3. As shown in Table 1, the derived real part of the RI for the non-absorbing SOA is  $1.584 \pm 0.015$  and  $1.551 \pm 0.011$  at the wavelength of 405 and 660 nm, respectively.

For the weakly absorbing SOA, the number mode average mobility diameter of the AAC-selected particles was  $202.91$  nm and the total number concentration was  $421 \pm 12$   $\text{cm}^{-3}$ . The corresponding mean extinction coefficients were  $33.45 \pm 0.50$   $\text{Mm}^{-1}$  and  $5.73 \pm 0.09$   $\text{Mm}^{-1}$  at 405 and 660 nm, respectively. The measured absorption coefficient at 405 nm was  $3.69 \pm 0.18$   $\text{Mm}^{-1}$ . By combining the measured particle size distribution with the absorption and extinction coefficients, the RI of the weakly absorbing SOA particles was retrieved using the method in Section 2.3. As shown in Table 1, the derived RIs are  $1.738 (\pm 0.021) + 0.0316 (\pm 0.0018) i$  and  $1.586 \pm 0.011$  at 405 and 660 nm, respectively. Our retrieved imaginary part ( $k$ ) of the weakly absorbing SOA at 405 nm is within the range of the imaginary part (0.005–0.45) for brown carbon as summarized by Wang et al. (2014).

There is a clear difference between the retrieved real components ( $n$ ) for the non-absorbing ( $1.738 \pm 0.021$ ) and weakly absorbing ( $1.584 \pm 0.015$ ) SOA at the wavelength of 405 nm, but this difference is less significant



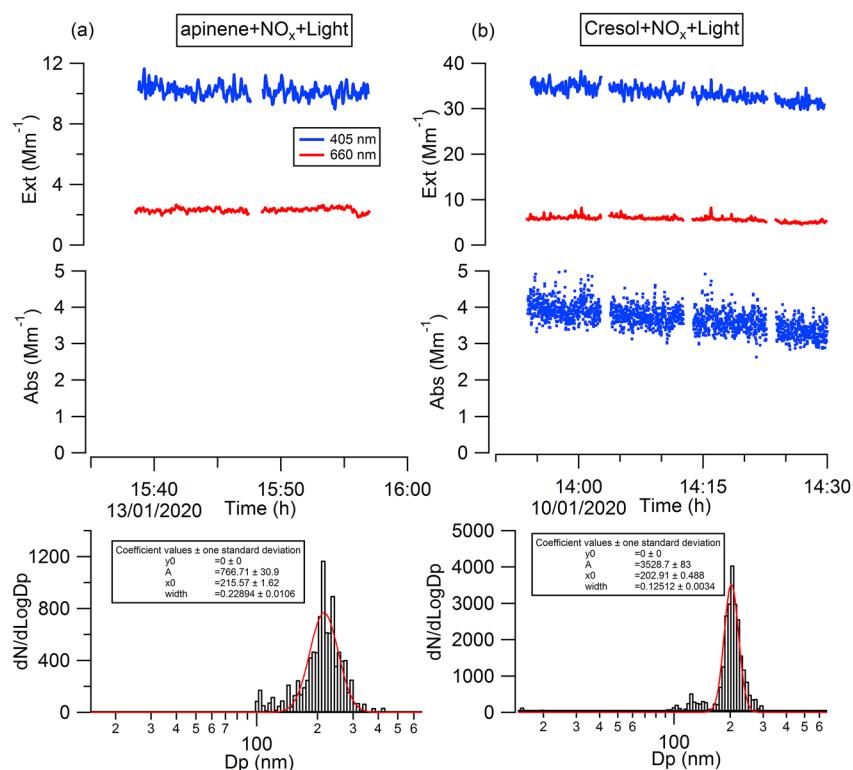


**Figure 3.** Optical properties and particle size distribution of the AAC-Selected particles from: (a) the non-absorbing SOA with the precursor of  $\alpha$ -pinene and  $\text{NO}_x$ , and (b) weakly absorbing SOA with the precursor of cresol and  $\text{NO}_x$ .

(less than 2.5%) at the wavelength of 660 nm. As neither the non-absorbing SOA nor weakly absorbing SOA experiments demonstrate any absorption at the 660 nm wavelength, our results imply that a single RI may be sufficient for simulating the optical properties of SOA particles at long visible wavelengths. Previous work reporting core-shell Mie calculations for coated BC particles have assumed a refractive index of  $1.5 + 0i$  for the non-BC components (Liu et al., 2017; Schwarz et al., 2008; Taylor et al., 2015). This assumed RI for coatings in previous work is not too dissimilar to the best-fit  $n$  from our analysis at the 660 nm wavelength and may be sufficient for simulating the optical properties of coated BC particles at this wavelength, but is likely not a suitable assumption for calculations pertaining to short visible wavelengths when the coating comprises brown carbon components. Moreover, the value for  $k$  needs careful consideration at these short wavelengths. More studies are needed for SOA of different compositions to ascertain the generality of whether a single refractive index may be ascribed to SOA optical properties at the  $\sim 660$  nm wavelength.

### 3.2. Refractive Index of BC

Figure 4 shows the evolving gas phase composition, particle size distribution, and optical properties following BC injection and then the formation of organic coatings. The size distribution of the bare BC particles shows a single

**Table 1**  
Derived Refractive Index of Pure SOA and Black Carbon at the Wavelength of 405 and 660 nm

Compounds	$\lambda = 405 \text{ nm}$		$\lambda = 660 \text{ nm}$	
	$n$	$k$	$n$	$k$
SOA_ $\alpha$ -pinene	$1.584 \pm 0.015$	—	$1.551 \pm 0.011$	—
SOA_Cresol	$1.738 \pm 0.021$	$0.0316 \pm 0.0018$	$1.586 \pm 0.011$	—
Bare BC_Experiment 1	$1.816 \pm 0.169$	$0.624 \pm 0.019$	—	—
Bare BC_Experiment 2	$1.923 \pm 0.202$	$0.656 \pm 0.022$	—	—

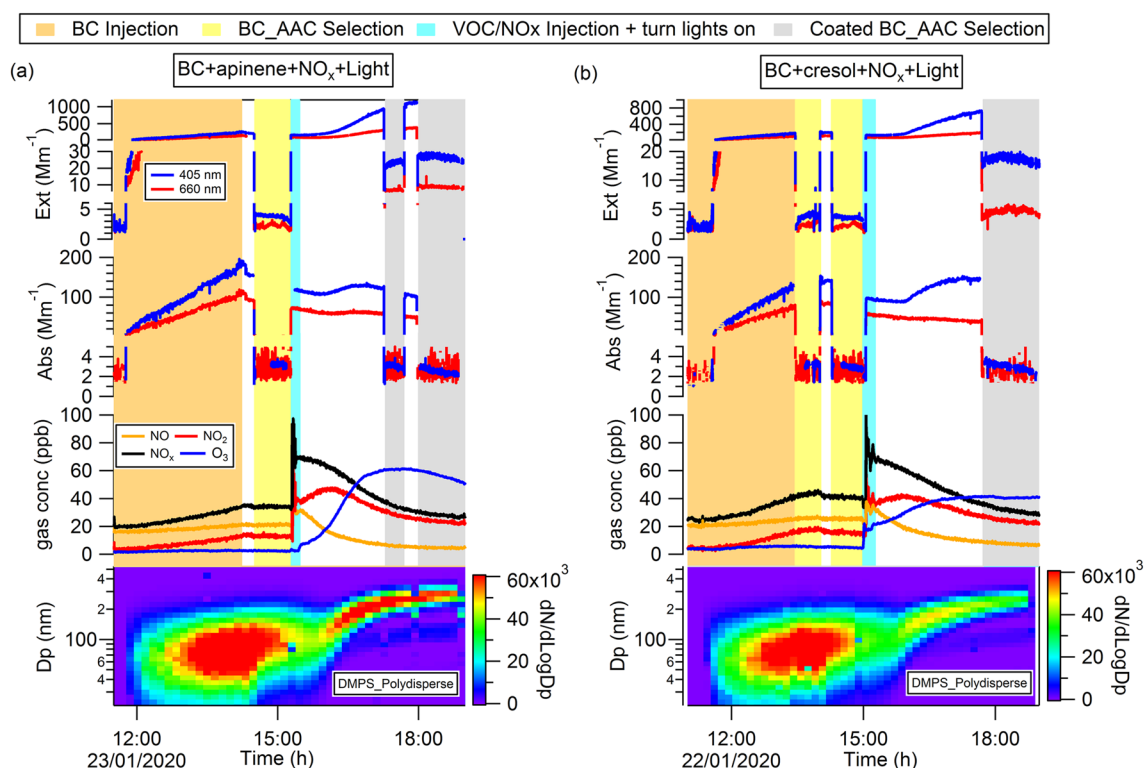


**Figure 4.** Evolution of: (a) the non-absorbing organics with the  $\alpha$ -pinene precursor and  $\text{NO}_x$ , and (b) weakly absorbing organics with the precursor of cresol and  $\text{NO}_x$ , condensing to pure BC particles. The acronyms Abs, Ext and  $D_p$  are absorption coefficient, extinction coefficient and mobility diameter of the particles, respectively.

mode with a number mode mobility diameter of 63 nm. After the precursors were injected into the chamber and the lights were switched on, the organics condense onto the BC particles and the size of the coated BC particles increased to a stable size of 281 and 256 nm in the non- and weakly absorbing SOA coating experiments respectively. For both experiments, the absorption and extinction coefficients increased with the injection time as the number concentration of BC in the chamber increases. After completion of BC injection, subsequent injection of the SOA precursors, and the illumination of the chamber using lights, the particle size showed only a slight increase (the number mode mobility diameter increased to 75 and 72 nm for non- and weakly absorbing SOA coating experiments respectively.) during the first 30 min. Simply, any organic species formed from the photoinitiated reaction had not had sufficient time to partition into the condensed phase in significant amounts. During this 30-min period, the absorption coefficient decreased slightly and this reduction is likely caused by particle losses to the chamber walls, while the extinction coefficient was stable which probably arises from the small increase in particle size counteracting the effect of particle losses; we highlight that extinction cross-sections are more sensitive to particle size than absorption cross-sections. After  $\sim 1$  hr following the chamber lights turning on, the particle size increases as BC particles become coated with SOA, and the extinction coefficient increases markedly for both non- and weakly absorbing SOA coating experiments. For the non-absorbing SOA coating, the absorption coefficient at 405 nm shows initially an increase followed by a slow decrease on longer timescales. For the absorbing SOA coating experiments, a monotonic increase in the 405-nm absorption coefficient is observed. The different trends in the absorption for these two experiments are probably due to the different intensive optical properties (i.e., the refractive indices) of the organic coatings. The absorption of the formed BrC at 405 nm could further enhance the absorption of the coated BC particles. In addition, the 660-nm absorption coefficient is decreasing for the absorbing SOA coating experiments. This is probably due to the wall loss of BC particles while red absorption is driven by BC mass. Although the mass-normalized optical cross-sections (Mass Absorption Cross-section (MAC) or Mass Extinction Cross-section (MEC)) can account for the wall loss effect, we are unable to provide this information in our study. The AMS was solely used for measuring polydisperse aerosols, and we lack the specific mass concentration of organics specifically during the size-selection period, which is essential for deriving the MAC and MEC.

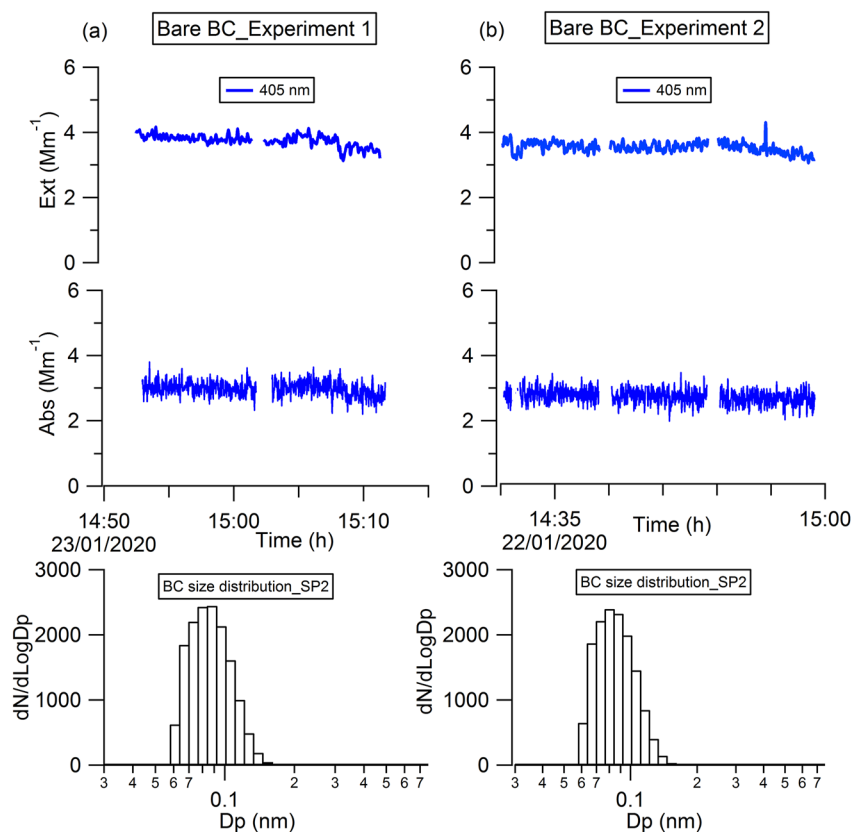


**Figure 5.** Optical properties and particle size distribution of the AAC-Selected bare BC particles.

Initially, the objective of this study was to determine the RI of bare BC particles at both 405 and 660 nm. However, in our attempts to increase the concentration of BC particles in order to obtain a signal at 660 nm, the CRDS signal at 405 nm exceeded the maximum threshold. Consequently, we were only able to obtain data at 405 nm. In both experiments, the signal-to-noise ratio in the optical measurements at the wavelength of 660 nm for AAC-selected BC particles is not adequate for RI retrievals, and only the RI of the bare BC particles at 405 nm is reported here. After completion of BC injection into the chamber, the SP2 and EXSCALABAR were used to measure the BC size distribution and the absorption and extinction coefficient of the AAC-selected aerosols. To maximize the absorption signal for the AAC-selected aerosol sample, the particle aerodynamic size distribution was first scanned to find the volume mode aerodynamic diameter. Then, the AAC was set to classify particles at this diameter for the downstream measurements. Since BC particles are non-spherical, the mobility size measured by SMPS is larger than its volume equivalent diameter. Therefore, the size distribution of the BC particles measured by the SP2 was used in the following RI retrieval calculations and this necessitated assuming the material density of soot ( $1.8 \text{ g cm}^{-3}$ , Taylor et al. (2014)). As mentioned in Section 2.3, we acknowledge that our choice in using Mie theory (which strictly applies to homogeneous spheres only) to retrieve the refractive indices of soot particles likely gives rise to errors in our retrieved RI values. However, the aim of this work is to derive effective RI values for use in climate models, which mostly rely on Mie theory-based models.

Figure 5 presents the particle absorption coefficient, extinction coefficient and the average size distribution of bare BC particles during an AAC size-selection period. For the non-absorbing SOA coating experiment (Figure 5a, denoted as Experiment 1 in Table 1), the size-selected BC particles had number mode optical diameter of  $80.23 \text{ nm}$  with total number concentration of  $603 \pm 14 \text{ cm}^{-3}$ . The corresponding mean absorption and extinction coefficient at 405 nm are  $2.98 \pm 0.15 \text{ Mm}^{-1}$  and  $3.75 \pm 0.06 \text{ Mm}^{-1}$ , respectively. For the weakly absorbing SOA coating experiment (Figure 5b, denoted as Experiment 2 in Table 1), the size-selected BC particles had a modal optical diameter of  $79.13 \text{ nm}$  with total number concentration of  $575 \pm 13 \text{ cm}^{-3}$ . The corresponding mean absorption and extinction coefficient at 405 nm are  $2.74 \pm 0.14 \text{ Mm}^{-1}$  and  $3.54 \pm 0.05 \text{ Mm}^{-1}$ , respectively. The retrieved RI values for the bare BC particles are summarized in Table 1. The derived RI at an optical wavelength

of 405 nm for the bare BC particles is  $1.816 (\pm 0.169) + 0.624 (\pm 0.019) i$  and  $1.923 (\pm 0.202) + (0.656 \pm 0.022) i$  for Experiment 1 and Experiment 2, respectively, with the mean value of  $1.870 (\pm 0.132) + 0.640 (\pm 0.015) i$ . The imaginary parts of the RI derived in the two experiments are consistent and the real parts of the derived RI are comparable and within the experiment uncertainties. To date, the most commonly assumed RI of BC particles in models and numerical studies is that recommended by Bond and Bergstrom (2006b), who recommended a RI of  $1.97 + 0.79i$  for visible and near infrared wavelengths. This recommended value is for void-free carbon and was obtained by comprehensive considerations of the reported RIs of BC from several different experimental studies. Black carbon in the atmosphere is rarely void-free, and instead a likely range of RIs ( $1.75 + 0.63i$  to  $1.97 + 0.79i$ ) was suggested by Bond and Bergstrom (2006b) for light-absorbing carbon. This RI range is further supported by our study as the RI of BC derived in our study, using an authentic real-world soot source, was within this range.

### 3.3. Optical Properties of Coated BC Particles: Models Results Testing

The chamber was used to coat BC particles to enable critical evaluation of different models of the optical properties for mixed particles. Models used included: (a) external mixing of Mie particles; (b) core-shell Mie theory; Mie theory calculations of particles for which the effective refractive index is described by (c) a linear volume weighting mixing rule (henceforth referred to as the “volume mixing” model), or (d) effective medium approximations that include both Maxwell-Garnett (Maxwell Garnett, 1906) and Bruggeman’s rule (Bruggeman, 2006). For the external mixing model, BC and non-BC components contribute independently to the total scattering and absorption. For the core-shell simulation, BC is enveloped by non-BC materials in a spherical core-shell arrangement, allowing the core-shell (coated sphere) Mie model to be applied. For the homogeneous mixing model, the effective RI of the coated particles is calculated assuming a volume weighted average based on the RI of each component. For the effective medium approximation simulations, the Maxwell-Garnett or Bruggemann mixing rules were applied. The description of the model calculations is provided in Section S2 in Supporting Information S1.

During the coating experiments, the coating materials increase with the aging time. Previous studies demonstrate that the absorption enhancement of BC particle in the ambient is depends on its coating state (Cappa et al., 2019), and the influence of coatings on BC absorption should be treated as a source and regionally specific parameter in climate models (Liu et al., 2015). To test the models with varying coating ratio of BC particles, particles at different aging time were selected by the AAC for investigation. Figure S1 in Supporting Information S1 presents the normalized average mass spectra of pure SOAs during the period used for deriving their RI values, as well as the normalized average mass spectra of the coating organics of the coated BC particles during the investigated period, along with the differences between them. Notably, there is minimal variation observed in the chemical composition of the SOAs generated in the presence and absence of BC particles. Furthermore, the stability of O/C and f44 values in the bulk aerosols throughout the investigated coating ratio period (shown in Figure S2 in Supporting Information S1) further supports the applicability of the RI derived from the pure SOAs to the coating organics of the coated BC particles. In addition, even though the RI of bare BC particles obtained from the non-irradiation experiments, it can still be applied to simulate the coated BC particles formed under irradiation. This is because the air inside the chamber is thoroughly cleansed with low concentrations of both gases and particles prior to injection, and the coatings on the bare BC particles emitted from the diesel engine are eliminated by a catalytic stripper. We are unaware of any studies that show modification of bare BC particles by sunlight (or light sources that mimic actinic flux) when particles exist in an environment devoid of pollutants that might undergo photochemical conversion at particle surfaces. For the coating ratio ( $CR = D_p/D_c$ ) calculation, the volume equivalent diameter of the BC core ( $D_c$ ) was directly measured from the incandescence signal of the SP2, while the diameter of the entire particle ( $D_p$ ) was measured by the SMPS ( $D_{p,SMPS}$ ) or the scattering signal of the SP2 ( $D_{p,SP2}$ ). Although pure BC particles are non-spherical, after being coated with a large amounts of organic material, the morphology has been observed to tend to spherical (Hu et al., 2021b), and the mobility diameter measured by the SMPS can be assumed to be equivalent to the volume equivalent diameter (DeCarlo et al., 2004). In this study, we compared calculations of the aerosol optical properties using CR calculated by  $D_{p,SMPS}/D_c$  (denoted as  $CR_{SMPS}$ ) and  $D_{p,SP2}/D_c$  (denoted as  $CR_{SP2}$ ).

A time series of absorption coefficient, extinction coefficient and single scattering albedo (SSA) of the AAC size-selected particles is presented in Figure 6, along with the average number concentration and the calculated average coating ratio for 7 different aging time periods (gray shaded area). For both experiments, particle number

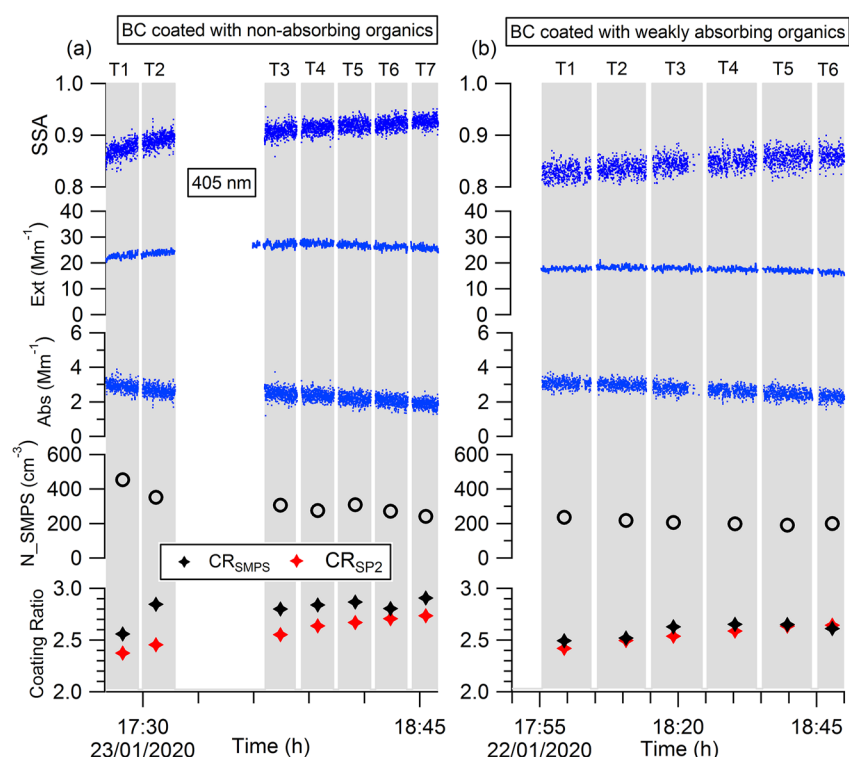


**Figure 6.** Optical properties, number concentration and coating ratio of: (a) BC coated with non-absorbing organics, and (b) BC coated with weakly absorbing organics.

concentration decreased with the aging time, because particles were lost to the walls of the chamber. As expected, the coating ratio increased with the aging time as more organic material condensed onto the particles. As the absorption is driven by BC mass concentration, losing particles to the chamber walls will decrease the measured absorption coefficient. Meanwhile, the extinction cross section of a particle is particularly sensitive to the particle size. Therefore, although the particle number concentration decreased, the extinction coefficient still increased with aging time as the particles grew larger. These differing trends in extinction and absorption coefficient lead to an increase in the single scattering albedo (SSA) with aging time, implying the coated BC particles become more scattering with more condensed materials. For BC coated with non-absorbing organics (Figure 6a), CR<sub>SMPS</sub> was larger than CR<sub>SP2</sub> throughout the experiment. This is because, as the particles are non-spherical, the mobility size measured by the SMPS is larger than the volume equivalent diameter measured by the SP2. Meanwhile, for BC coated with weakly absorbing organics (Figure 6b), CR<sub>SMPS</sub> agrees well with CR<sub>SP2</sub> throughout the experiment, implying that the particles are approximately spherical. Our results show that particles with an approximately spherical morphology are formed for BC particles coated in cresol-derived SOA, in stark contrast to those coated in the  $\alpha$ -pinene derived SOA, which may reflect the physicochemical properties of the SOA produced.

Measured and modeled optical properties for the coated BC particles with different coating ratios are presented in Figure 7. We note that, although a more representative input of mixing state could have been used as input to model calculations by applying a more rigorous treatment of the SP2 measurement data (see Taylor et al. (2020)), the mixing state of the coated BC particles was not accounted in this study, because the scope of this work is to quantify effective refractive indices for BC particles using tracer variables currently available to common climate models (i.e., the typical observables of particle size distribution and pure component refractive indices). The particle-to-particle variability could indeed provide an insight into mixing state, however in this instance the ability to do this is limited by the measurement precision of the SP2 incandescence detection channel. While we are confident in the mean core size of the particles, it is impossible to disentangle real physical variability from this measurement precision. Note that while this was assessed in previous papers such as Yu et al. (2020), this was through using data at multiple monodisperse size selections and observing the trends within the two-dimensional data space, which is not possible here. For BC coated with non-absorbing organics (Figure 7a), when using CR<sub>SP2</sub>,

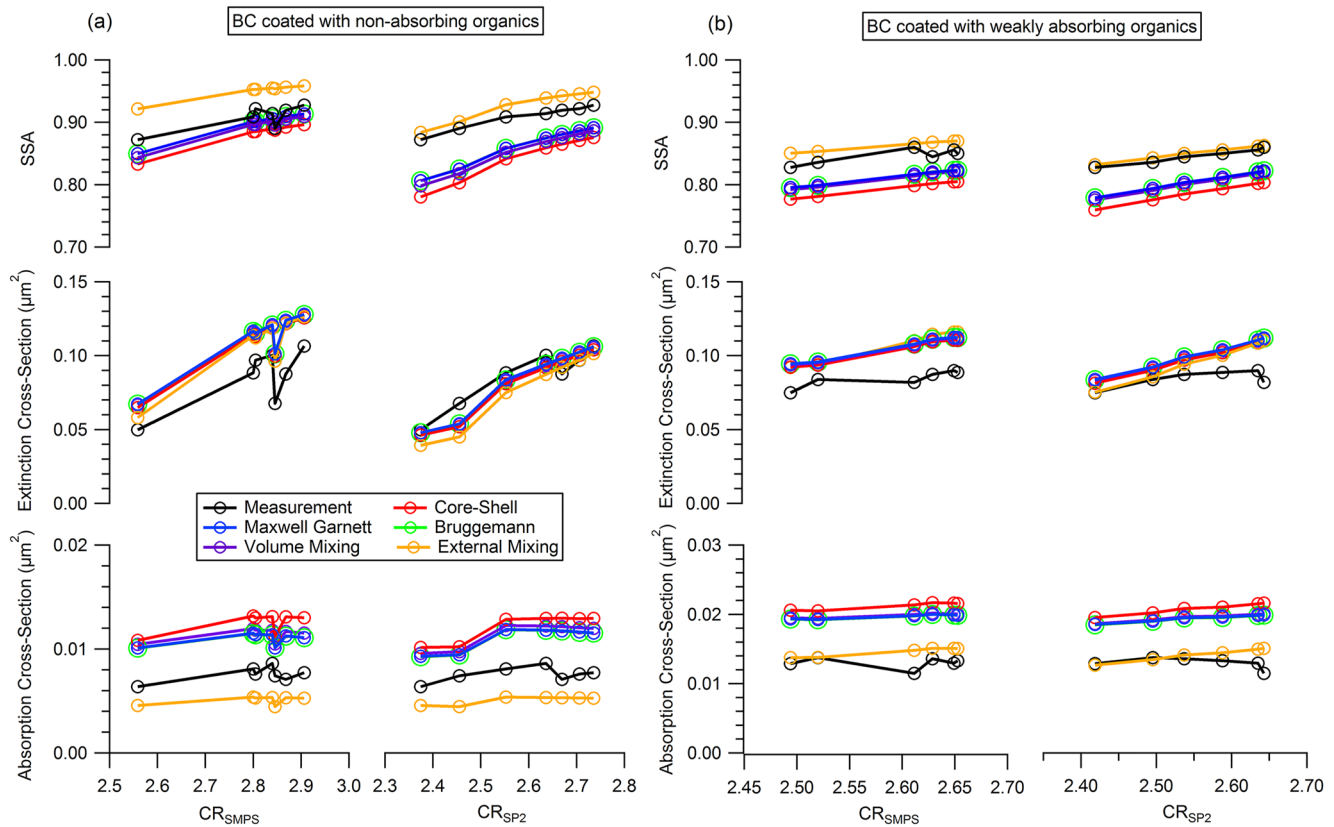


**Figure 7.** Comparison of the simulated optical properties from different models with the measurement of the BC particles coated with: (a) non-absorbing organics, and (b) weakly absorbing organics.

the simulated extinction cross-section agrees well with the measurement across all coating ratios. However, the models overestimated the simulated extinction cross-section by 17.8%–47.3% when using  $CR_{SMPs}$ . Modeled and measured absorption cross-sections are in poor agreement regardless of which CR metric is chosen. The core-shell, volume mixing rule, and effective medium approximation models significantly over-estimate absorption, while the external mixing model under-estimates absorption. For example, for simulations using  $CR_{SP2}$  as the input, the core-shell model over-estimated absorption by 37.7%–70.4%, the volume mixing model over-estimated by 31.1%–72.0% and the effective medium approximation models over-estimated by 27.2%–66.2%, while the external mixing model under-estimated by 24.8%–40.0%.

For BC coated with weakly absorbing organics (Figure 7b), the simulated extinction cross-sections agree well with each other when using the  $CR_{SMPs}$  as the coating ratio of BC particles, but over-estimate extinction by 11.7%–29.5%. For  $CR_{SP2}$  as an input to the optical model calculations, the simulation results from the external mixing model show good agreement with measurements for  $CR_{SP2}$  less than 2.5, but the difference between the simulations and measurements increases for larger coating ratios. For example, the calculated extinction cross-section is over-estimated by 30.8% for a  $CR_{SP2}$  of 2.65. For the absorption cross-section, the external mixing rule model is better than other models at reproducing the measurements. For example, for simulations using  $CR_{SP2}$ , the absorption cross-sections calculated assuming external mixing agree very well with the measured values for  $CR_{SP2}$  values less than 2.55, while other models over-estimate the absorption by 38.4%–43.7%. For  $CR_{SP2}$  values larger than 2.55, the difference between the external mixing model values and measured values increases as the coating grows, but this difference remains less than 31.6% and still performs better than models applying alternative mixing assumptions. For the SSA, the simulation results from the external mixing model when using  $CR_{SP2}$  show good agreement with measurements across the whole CR range. The good agreement of SSA between simulation and measurement at larger  $CR_{SP2}$  arises because the simulated absorption and extinction values are both overestimated to similar extents.

Although assuming external mixing is best for reproducing measurements in this work, there remain significant discrepancies, for thick coatings ( $CR > 2.5$ ) especially. Disagreement between measurements and simulations



has often been reported by previous studies. Liu et al. (2017) investigated the absorption enhancement of black carbon particles emitted from the same engine used here, except the particle-laden samples were not stripped of their VOC contents. The authors noted that the core-shell model over-estimated the absorption enhancement of the BC particles. They also found that the majority of BC from urban traffic sources is best described as externally mixed, which is consistent with our results from BC coated with weakly absorbing organics. Taylor et al. (2020) investigated the absorption enhancement of highly aged biomass burning aerosols and found that the homogeneous gray-sphere Mie model was only able to simulate the observed absorption enhancement by assuming an unrealistically low value of the BC refractive index. Additionally, the core-shell Mie model consistently underestimated the absorption enhancement at short visible wavelengths (405 nm), but these model predictions remained within the uncertainty of the measurements at wavelengths of 515 and 660 nm for acceptable ranges in BC refractive index. The core-shell model underestimated absorption enhancement in Taylor et al. (2020) but over-estimated the particle absorption in Liu et al. (2017) and our work. This difference may be due to the highly aged nature of the BC particles in the former study. There are a number of factors that could be responsible for the differences between measurements and the Mie model calculations. Schemes that assume all particles are spherical and are based on Mie theory are relatively simple to implement, but this representation of particle morphologies is too simplistic (Adachi et al., 2010). Fresh soot particles often exist in the form of aggregates composed of primary spherules with irregular geometries (Wentzel et al., 2003; Xiong and Friedlander, 2001), which increase the individual particle absorption cross sections because more of the soot surface is exposed to incident light. After aging in the atmosphere, the particles gain coatings and these may cause soot aggregates to collapse into a quasi-spherical shape (Corbin et al., 2023; Li et al., 2003). This could reduce absorption as less of the soot is exposed to light (Scarnato et al., 2013), or it could increase absorption due to stronger interactions between neighboring soot spherules (Liu et al., 2008). The relative importance of these two competing effects is wavelength dependent. Beeler and Chakrabarty (2022) introduced a single metric, the phase shift parameter ( $\rho_{BC}$ ), to encompass the complex diversity in size and morphology of BC aggregates. They found that  $\rho_{BC} > 1$  results in decreased absorption by BC, providing an explanation for the weaker absorption enhancements observed in certain regional BC compared to laboratory results of similar mixing state. In our previous study (Hu et al., 2021a), we calculated and discussed the shape factor of bare BC particles, including those emitted from the same engine examined in this study, across different sizes. However, the shape factor of the coated BC particles cannot be determined in this study due to the unknown density of the coating materials. Although the coating compositions and RI have been determined in this study, differences between measurements and simulations persist when considering mixed BC-SOA particles. This suggests that optical models must consider the particle morphology and particle-to-particle differences in composition to accurately capture the absorption enhancement of BC particles.

#### 4. Conclusions

During the Soot Aerodynamic Size Selection for Optical properties (SASSO) project, the Aerodynamic Aerosol Classifier is coupled with the EXSCALABAR instrument, enabling optical extinction and absorption measurements of an aerosol sample classified according to a single physical size. This approach is not subject to multiple charge artifacts that disadvantage approaches that use electrical mobility classification, which improves the subsequent RI retrieval using a Mie scattering theory model. The refractive index of pure black carbon from engine emission was investigated. The retrieved refractive indices of pure BC particles at 405 nm were  $1.870 (\pm 0.132) + 0.640 (\pm 0.015) i$ . Organic matter from both absorbing and non-absorbing chamber-generated secondary organic aerosol (SOA) were also studied. The determined refractive indices of non-absorbing SOA at 405 and 660 nm were  $1.584 \pm 0.015$  and  $1.551 \pm 0.011$ , respectively, while those for weakly absorbing SOA were  $1.738 (\pm 0.021) + 0.0316 (\pm 0.0018) i$  and  $1.586 \pm 0.011$ , at 405 and 660 nm respectively. Our results imply that a single RI may be sufficient for simulating the radiative forcing of SOA (including absorbing SOA) particles at the wavelength of 660 nm, with non-absorbing and weakly absorbing SOA shown to be non-absorbing at the wavelength of 660 nm and their real RI values are similar.

The non-absorbing and weakly absorbing organics condensed on to the BC particles in the chamber to test different models used to represent the optical properties of mixed particles in climate models. For the BC particles coated with non-absorbing organics, the simulated extinction cross-sections agree well with the measurements when using the optical diameter from the SP2 for coating ratio measurements. For BC particles coated with weakly absorbing organics, the extinction and absorption cross-sections simulated assuming external mixing

show good agreement with measurements when the coating ratio of BC particles is less than 2.5. For other conditions and despite well-characterized coating compositions and RIs, significant differences between the measurements and simulations were observed. This indicates that only knowing the equivalent diameter and component RIs is not sufficient for predicting the absorption of BC particles. It is necessary to consider additional factors such as morphology and particle-to-particle differences in mixing state to predict the absorption enhancement of BC particles.

## Conflict of Interest

The authors declare no conflicts of interest relevant to this study.

## Data Availability Statement

The dataset for this research is available at (Hu, 2023).

## Acknowledgments

This work was supported by the UK Natural Environment Research Council (NERC) (Grant Ref. NE/S00212x/1) and the Met Office, and received a trans-national activity funding from the European Union's Horizon 2020 research and innovation programme through the EUROCHAMP-2020 Infrastructure Activity under Grant Agreement No. 730997. Thanks to Catalytic Instruments for the loan of the catalytic stripper CS10. The authors declare there are no potential conflicts of interest.

## References

- Adachi, K., Chung, S. H., & Buseck, P. R. (2010). Shapes of soot aerosol particles and implications for their effects on climate. *Journal of Geophysical Research*, 115(D15), D15206. <https://doi.org/10.1029/2009JD012868>
- Adachi, K., Sedlacek, A. J., Kleinman, L., Springston, S. R., Wang, J., Chand, D., et al. (2019). Spherical tarball particles form through rapid chemical and physical changes of organic matter in biomass-burning smoke. *Proceedings of the National Academy of Sciences of the United States of America*, 116(39), 19336–19341. <https://doi.org/10.1073/pnas.1900129116>
- Alfarra, M. R., Hamilton, J. F., Wyche, K. P., Good, N., Ward, M. W., Carr, T., et al. (2012). The effect of photochemical ageing and initial precursor concentration on the composition and hygroscopic properties of  $\beta$ -caryophyllene secondary organic aerosol. *Atmospheric Chemistry and Physics*, 12(14), 6417–6436. <https://doi.org/10.5194/acp-12-6417-2012>
- Beeler, P., & Chakrabarty, R. K. (2022). Constraining the particle-scale diversity of black carbon light absorption using a unified framework. *Atmospheric Chemistry and Physics*, 22(22), 14825–14836. <https://doi.org/10.5194/acp-22-14825-2022>
- Bond, T. C., & Bergstrom, R. W. (2006a). Light absorption by carbonaceous particles: An investigative review. *Aerosol Science & Technology*, 40(1), 27–67. <https://doi.org/10.1080/02786820500421521>
- Bond, T. C., & Bergstrom, R. W. (2006b). Light absorption by carbonaceous particles: An investigative review. *Aerosol Science and Technology*, 40(1), 27–67. <https://doi.org/10.1080/02786820500421521>
- Bond, T. C., Doherty, S. J., Fahey, D. W., Forster, P. M., Bernsten, T., DeAngelo, B. J., et al. (2013). Bounding the role of black carbon in the climate system: A scientific assessment. *Journal of Geophysical Research: Atmospheres*, 118(11), 5380–5552. <https://doi.org/10.1002/jgrd.50171>
- Bruggeman, D. (2006). Berechnung Verschiedener Physikalischer Konstanten von Heterogenen Substanzen. I. Dielektrizitätskonstanten und Leitfähigkeiten der Mischkörper aus Isotropen Substanzen. *Annalen der Physik*, 416(7), 636–664. <https://doi.org/10.1002/andp.19354160705>
- Canagaratna, M. R., Jayne, J. T., Jimenez, J. L., Allan, J. D., Alfarra, M. R., Zhang, Q., et al. (2007). Chemical and microphysical characterization of ambient aerosols with the aerodyne aerosol mass spectrometer. *Mass Spectrometry Reviews*, 26(2), 185–222. <https://doi.org/10.1002/mas.20115>
- Cappa, C. D., Onasch, T. B., Massoli, P., Worsnop, D. R., Bates, T. S., Cross, E. S., et al. (2012). Radiative absorption enhancements due to the mixing state of atmospheric black carbon. *Science*, 337(6098), 1078–1081. <https://doi.org/10.1126/science.1223447>
- Cappa, C. D., Zhang, X., Russell, L. M., Collier, S., Lee, A. K. Y., Chen, C.-L., et al. (2019). Light absorption by ambient black and Brown carbon and its dependence on black carbon coating state for two California, USA, cities in winter and summer. *Journal of Geophysical Research: Atmospheres*, 124(3), 1550–1577. <https://doi.org/10.1029/2018JD029501>
- Cavalli, F., Viana, M., Yttri, K. E., Genberg, J., & Putaud, J. P. (2010). Toward a standardised thermal-optical protocol for measuring atmospheric organic and elemental carbon: The EUSAAR protocol. *Atmospheric Measurement Techniques*, 3(1), 79–89. <https://doi.org/10.5194/amt-3-79-2010>
- Corbin, J. C., Modini, R. L., & Gysel-Beer, M. (2023). Mechanisms of soot-aggregate restructuring and compaction. *Aerosol Science and Technology*, 57(2), 89–111. <https://doi.org/10.1080/02786826.2022.2137385>
- Cotterell, M. I., Orr-Ewing, A. J., Szpek, K., Haywood, J. M., & Langridge, J. M. (2019a). The impact of bath gas composition on the calibration of photoacoustic spectrometers with ozone at discrete visible wavelengths spanning the Chappuis band. *Atmospheric Measurement Techniques*, 12(4), 2371–2385. <https://doi.org/10.5194/amt-12-2371-2019>
- Cotterell, M. I., Szpek, K., Haywood, J. M., & Langridge, J. M. (2020). Sensitivity and accuracy of refractive index retrievals from measured extinction and absorption cross sections for mobility-selected internally mixed light absorbing aerosols. *Aerosol Science & Technology*, 54(9), 1034–1057. <https://doi.org/10.1080/02786826.2020.1757034>
- Cotterell, M. I., Szpek, K., Tiddeman, D. A., Haywood, J. M., & Langridge, J. M. (2021). Photoacoustic studies of energy transfer from ozone photoproducts to bath gases following Chappuis band photoexcitation. *Physical Chemistry Chemical Physics*, 23(1), 536–553. <https://doi.org/10.1039/D0CP05056C>
- Cotterell, M. I., Ward, G. P., Hibbins, A. P., Wilson, A., Haywood, J. M., & Langridge, J. M. (2019b). Optimizing the performance of aerosol photoacoustic cells using a finite element model. Part 2: Application to a two-resonator cell. *Aerosol Science & Technology*, 53(10), 1128–1148. <https://doi.org/10.1080/02786826.2019.1648749>
- Davies, N. W., Cotterell, M. I., Fox, C., Szpek, K., Haywood, J. M., & Langridge, J. M. (2018). On the accuracy of aerosol photoacoustic spectrometer calibrations using absorption by ozone. *Atmospheric Measurement Techniques*, 11(4), 2313–2324. <https://doi.org/10.5194/amt-11-2313-2018>
- DeCarlo, P. F., Slowik, J. G., Worsnop, D. R., Davidovits, P., & Jimenez, J. L. (2004). Particle morphology and density characterization by combined mobility and aerodynamic diameter measurements. Part 1: Theory. *Aerosol Science & Technology*, 38(12), 1185–1205. <https://doi.org/10.1080/027868290903907>

- Fierce, L., Bond, T. C., Bauer, S. E., Mena, F., & Riemer, N. (2016). Black carbon absorption at the global scale is affected by particle-scale diversity in composition. *Nature Communications*, 7(1), 12361. <https://doi.org/10.1038/ncomms12361>
- Haywood, J. M., Abel, S. J., Barrett, P. A., Bellouin, N., Blyth, A., Bower, K. N., et al. (2021). The CLoud–aerosol–radiation interaction and forcing: Year 2017 (CLARIFY-2017) measurement campaign. *Atmospheric Chemistry and Physics*, 21(2), 1049–1084. <https://doi.org/10.5194/acp-21-1049-2021>
- Haywood, J. M., & Shine, K. P. (1995). The effect of anthropogenic sulfate and soot aerosol on the clear sky planetary radiation budget. *Geophysical Research Letters*, 22(5), 603–606. <https://doi.org/10.1029/95GL00075>
- Hu, D. (2023). Data for the manuscript entitled Refractive index of engine-emitted black carbon and the influence of organic coatings on optical properties submitted to the Journal of Geophysical Research-Atmospheres. [Dataset]. Figshare. <https://doi.org/10.48420/22716904.v1>
- Hu, D., Alfarra, M. R., Szpek, K., Langridge, J. M., Cotterell, M. I., Belcher, C., et al. (2021a). Physical and chemical properties of black carbon and organic matter from different combustion and photochemical sources using aerodynamic aerosol classification. *Atmospheric Chemistry and Physics*, 21(21), 16161–16182. <https://doi.org/10.5194/acp-21-16161-2021>
- Hu, K., Liu, D., Tian, P., Wu, Y., Deng, Z., Wu, Y., et al. (2021b). Measurements of the diversity of shape and mixing state for ambient black carbon particles. *Geophysical Research Letters*, 48(17), e2021GL094522. <https://doi.org/10.1029/2021GL094522>
- Johnson, B. T., Haywood, J. M., Langridge, J. M., Darbyshire, E., Morgan, W. T., Szpek, K., et al. (2016). Evaluation of biomass burning aerosols in the HadGEM3 climate model with observations from the SAMBBA field campaign. *Atmospheric Chemistry and Physics*, 16(22), 14657–14685. <https://doi.org/10.5194/acp-16-14657-2016>
- Knox, A., Evans, G. J., Brook, J. R., Yao, X., Jeong, C. H., Godri, K. J., et al. (2009). Mass absorption cross-section of ambient black carbon aerosol in relation to chemical age. *Aerosol Science and Technology*, 43(6), 522–532. <https://doi.org/10.1080/02786820902777207>
- Li, J., Pósfai, M., Hobbs, P. V., & Buseck, P. R. (2003). Individual aerosol particles from biomass burning in southern Africa: 2, compositions and aging of inorganic particles. *Journal of Geophysical Research*, 108(D13). <https://doi.org/10.1029/2002JD002310>
- Liu, S., Aiken, A. C., Gorkowski, K., Dubey, M. K., Cappa, C. D., Williams, L. R., et al. (2015). Enhanced light absorption by mixed source black and brown carbon particles in UK winter. *Nature Communications*, 6(1), 8435. <https://doi.org/10.1038/ncomms9435>
- Liu, D., Flynn, M., Gysel, M., Targino, A., Crawford, I., Bower, K., et al. (2010). Single particle characterization of black carbon aerosols at a tropospheric alpine site in Switzerland. *Atmospheric Chemistry and Physics*, 10(15), 7389–7407. <https://doi.org/10.5194/acp-10-7389-2010>
- Liu, D., He, C., Schwarz, J. P., & Wang, X. (2020a). Lifecycle of light-absorbing carbonaceous aerosols in the atmosphere. *NPJ Climate and Atmospheric Science*, 3(1), 40. <https://doi.org/10.1038/s41612-020-00145-8>
- Liu, L., Mishchenko, M. I., & Patrick Arnott, W. (2008). A study of radiative properties of fractal soot aggregates using the superposition T-matrix method. *Journal of Quantitative Spectroscopy and Radiative Transfer*, 109(15), 2656–2663. <https://doi.org/10.1016/j.jqsrt.2008.05.001>
- Liu, D., Whitehead, J., Alfarra, M. R., Reyes-Villegas, E., Spracklen, D. V., Reddington, C. L., et al. (2017). Black-carbon absorption enhancement in the atmosphere determined by particle mixing state. *Nature Geoscience*, 10(3), 184–188. <https://doi.org/10.1038/ngeo2901>
- Liu, F., Yon, J., Fuentes, A., Lobo, P., Smallwood, G. J., & Corbin, J. C. (2020b). Review of recent literature on the light absorption properties of black carbon: Refractive index, mass absorption cross section, and absorption function. *Aerosol Science and Technology*, 54(1), 33–51. <https://doi.org/10.1080/02786826.2019.1676878>
- Martins, J. V., Artaxo, P., Lioussé, C., Reid, J. S., Hobbs, P. V., & Kaufman, Y. J. (1998). Effects of black carbon content, particle size, and mixing on light absorption by aerosols from biomass burning in Brazil. *Journal of Geophysical Research*, 103(D24), 32041–32050. <https://doi.org/10.1029/98JD02593>
- Maxwell Garnett, J. C. (1906). Colours in metal glasses, in metallic films, and in metallic solutions. II. *Philosophical Transactions of the Royal Society of London, Series A*, 205, 237–288.
- Moteki, N., & Kondo, Y. (2007). Effects of mixing state on black carbon measurements by laser-induced incandescence. *Aerosol Science & Technology*, 41(4), 398–417. <https://doi.org/10.1080/02786820701199728>
- Moteki, N., Kondo, Y., & Nakamura, S.-I. (2010). Method to measure refractive indices of small nonspherical particles: Application to black carbon particles. *Journal of Aerosol Science*, 41(5), 513–521. <https://doi.org/10.1016/j.jaerosci.2010.02.013>
- Nakayama, T., Matsumi, Y., Sato, K., Imamura, T., Yamazaki, A., & Uchiyama, A. (2010). Laboratory studies on optical properties of secondary organic aerosols generated during the photooxidation of toluene and the ozonolysis of  $\alpha$ -pinene. *Journal of Geophysical Research*, 115(D24). <https://doi.org/10.1029/2010jd014387>
- Olfert, J. S., & Collings, N. (2005). New method for particle mass classification—The Couette centrifugal particle mass analyzer. *Journal of Aerosol Science*, 36(11), 1338–1352. <https://doi.org/10.1016/j.jaerosci.2005.03.006>
- Olfert, J. S., Reavell, K. S., Rushton, M. G., & Collings, N. (2006). The experimental transfer function of the Couette centrifugal particle mass analyzer. *Journal of Aerosol Science*, 37(12), 1840–1852. <https://doi.org/10.1016/j.jaerosci.2006.07.007>
- Peña, O., & Pal, U. (2009). Scattering of electromagnetic radiation by a multilayered sphere. *Computer Physics Communications*, 180(11), 2348–2354. <https://doi.org/10.1016/j.cpc.2009.07.010>
- Pereira, K. L., Dunmore, R., Whitehead, J., Alfarra, M. R., Allan, J. D., Alam, M. S., et al. (2018). Technical note: Use of an atmospheric simulation chamber to investigate the effect of different engine conditions on unregulated VOC-IVOC diesel exhaust emissions. *Atmospheric Chemistry and Physics*, 18(15), 11073–11096. <https://doi.org/10.5194/acp-18-11073-2018>
- IPCC. (2022). *Climate change 2022: Impacts, adaptation, and vulnerability. Contribution of working group II to the Sixth Assessment Report of the Intergovernmental Panel on climate change*. In H.-O. Pörtner, D. C. Roberts, M. Tignor, E. S. Poloczanska, K. Mintenbeck, et al. (Eds.), Cambridge University Press, (p. 3056). <https://doi.org/10.1017/9781009325844>
- Scarnato, B. V., Vahidinia, S., Richard, D. T., & Kirchstetter, T. W. (2013). Effects of internal mixing and aggregate morphology on optical properties of black carbon using a discrete dipole approximation model. *Atmospheric Chemistry and Physics*, 13(10), 5089–5101. <https://doi.org/10.5194/acp-13-5089-2013>
- Schwarz, J. P., Spackman, J. R., Fahey, D. W., Gao, R. S., Lohmann, U., Stier, P., et al. (2008). Coatings and their enhancement of black carbon light absorption in the tropical atmosphere. *Journal of Geophysical Research*, 113(D3), D03203. <https://doi.org/10.1029/2007JD009042>
- Sedlacek, A. J., III, Lewis, E. R., Onasch, T. B., Zuidema, P., Redemann, J., Jaffe, D., & Kleinman, L. I. (2022). Using the black carbon particle mixing state to characterize the Lifecycle of biomass burning aerosols. *Environmental Science & Technology*, 56(20), 14315–14325. <https://doi.org/10.1021/acs.est.2c03851>
- Shetty, N., Beeler, P., Paik, T., Brechtel, F. J., & Chakrabarty, R. K. (2021). Bias in quantification of light absorption enhancement of black carbon aerosol coated with low-volatility brown carbon. *Aerosol Science and Technology*, 55(5), 539–551. <https://doi.org/10.1080/02786826.2021.1873909>
- Tavakoli, F., Symonds, J. P. R., & Olfert, J. S. (2014). Generation of a monodisperse size-classified aerosol independent of particle charge. *Aerosol Science & Technology*, 48(3), i–iv. <https://doi.org/10.1080/02786826.2013.877121>

- Taylor, J. W., Allan, J. D., Allen, G., Coe, H., Williams, P. I., Flynn, M. J., et al. (2014). Size-dependent wet removal of black carbon in Canadian biomass burning plumes. *Atmospheric Chemistry and Physics*, 14(24), 13755–13771. <https://doi.org/10.5194/acp-14-13755-2014>
- Taylor, J. W., Allan, J. D., Liu, D., Flynn, M., Weber, R., Zhang, X., et al. (2015). Assessment of the sensitivity of core/shell parameters derived using the single-particle soot photometer to density and refractive index. *Atmospheric Measurement Techniques*, 8(4), 1701–1718. <https://doi.org/10.5194/amt-8-1701-2015>
- Taylor, J. W., Wu, H., Szpek, K., Bower, K., Crawford, I., Flynn, M. J., et al. (2020). Absorption closure in highly aged biomass burning smoke. *Atmospheric Chemistry and Physics*, 20(19), 11201–11221. <https://doi.org/10.5194/acp-20-11201-2020>
- Wang, X., Heald, C. L., Ridley, D. A., Schwarz, J. P., Spackman, J. R., Perring, A. E., et al. (2014). Exploiting simultaneous observational constraints on mass and absorption to estimate the global direct radiative forcing of black carbon and brown carbon. *Atmospheric Chemistry and Physics*, 14(20), 10989–11010. <https://doi.org/10.5194/acp-14-10989-2014>
- Wentzel, M., Gorzawski, H., Naumann, K. H., Saathoff, H., & Weinbruch, S. (2003). Transmission electron microscopical and aerosol dynamical characterization of soot aerosols. *Journal of Aerosol Science*, 34(10), 1347–1370. [https://doi.org/10.1016/S0021-8502\(03\)00360-4](https://doi.org/10.1016/S0021-8502(03)00360-4)
- Wu, H., Taylor, J. W., Langridge, J. M., Yu, C., Allan, J. D., Szpek, K., et al. (2021). Rapid transformation of ambient absorbing aerosols from West African biomass burning. *Atmospheric Chemistry and Physics*, 21(12), 9417–9440. <https://doi.org/10.5194/acp-21-9417-2021>
- Xiong, C., & Friedlander, S. K. (2001). Morphological properties of atmospheric aerosol aggregates. *Proceedings of the National Academy of Sciences of the United States of America*, 98(21), 11851–11856. <https://doi.org/10.1073/pnas.211376098>
- Yu, C., Liu, D., Broda, K., Joshi, R., Olfert, J., Sun, Y., et al. (2020). Characterising mass-resolved mixing state of black carbon in Beijing using a morphology-independent measurement method. *Atmospheric Chemistry and Physics*, 20(6), 3645–3661. <https://doi.org/10.5194/acp-20-3645-2020>
- Zhang, Y., Favez, O., Canonaco, F., Liu, D., Močnik, G., Amodeo, T., et al. (2018). Evidence of major secondary organic aerosol contribution to lensing effect black carbon absorption enhancement. *NPJ Climate and Atmospheric Science* 1(1), 47. <https://doi.org/10.1038/s41612-018-0056-2>
- Zhang, X., Mao, M., Yin, Y., & Wang, B. (2017). Absorption enhancement of aged black carbon aerosols affected by their microphysics: A numerical investigation. *Journal of Quantitative Spectroscopy and Radiative Transfer*, 202, 90–97. <https://doi.org/10.1016/j.jqsrt.2017.07.025>
- Zuidema, P., Redemann, J., Haywood, J., Wood, R., Piketh, S., Hipondoka, M., & Formenti, P. (2016). Smoke and clouds above the Southeast Atlantic: Upcoming field campaigns probe absorbing aerosol's impact on climate. *Bulletin of the American Meteorological Society*, 97(7), 1131–1135. <https://doi.org/10.1175/bams-d-15-00082.1>